Observed Boundary Layer Wind Structure and Balance in the Hurricane Core. Part II: Hurricane Mitch

JEFFREY D. KEPERT

Bureau of Meteorology Research Centre, Melbourne, Australia

(Manuscript received 27 April 2005, in final form 12 December 2005)

ABSTRACT

Part I of this paper presented a detailed analysis of the boundary layer of Hurricane Georges (1998), based mainly on the newly available high-resolution GPS dropsonde data. Here, similar techniques and data are used to study Hurricane Mitch (1998). In contrast to Hurricane Georges, the flow in the middle to upper boundary layer near the eyewall is found to be strongly supergradient, with the imbalance being statistically significant. The reason for the difference is shown to be the different radial structure of the storms, in that outside of the radius of maximum winds, the wind decreases much more quickly in Mitch than in Georges. Hurricane Mitch was close to inertially neutral at large radius, with a strong angular momentum gradient near the radius of maximum winds. Kepert and Wang predict strongly supergradient flow in the upper boundary layer near the radius of maximum winds in this situation; the observational analysis is thus in good agreement with their theory. The wind reduction factor (i.e., ratio of a near-surface wind speed to that at some level further aloft) is found to increase inward toward the radius of maximum winds, in accordance with theoretical predictions and the analysis by Franklin et al. Marked asymmetries in the boundary layer wind field and in the eyewall convection are shown to be consistent with asymmetric surface friction due to the storm's proximity to land, rather than to motion. The boundary layer flow was simulated using Kepert and Wang's model, forced by the observed storm motion, radial profile of gradient wind, and coastline position; and good agreement with the observations was obtained.

1. Introduction

Kepert (2006, hereafter Part I) presented an analysis of GPS dropsonde wind data from the boundary layer (BL) of the core of Hurricane Georges. One purpose of that paper was to exploit the unique characteristics of this relatively new data source to thoroughly document the wind structure in the BL of the tropical cyclone (TC) core. A second aim was to test the theoretical predictions of Kepert (2001, henceforth K01) and Kepert and Wang (2001, henceforth KW01), made with the aid of three-dimensional analytic and numerical models respectively, which diagnose the boundary layer flow as the response to a prescribed forcing pressure field representative of a tropical cyclone. These models and predictions are summarized in Part I.

It was found in Hurricane Georges (Part I) that the theoretical predictions regarding the spatial variability of the wind reduction factor (WRF; the ratio of a near-surface wind speed to that above the boundary layer) were well supported by the data, that the spatial variability in the general shape of the vertical wind profile was consistent with the theory, but that the flow in the upper part of the BL was not supergradient. However, it was also shown that the particular structure of Hurricane Georges would be expected to lead to only weakly supergradient flow in the upper BL near the radius of maximum winds (RMW) in KW01's model, so this difference was not strongly at variance with the theory.

Here, similar analysis techniques are applied to Hurricane Mitch of 1998. The results will be seen to be in marked contrast to those obtained in Hurricane Georges. In Mitch, there is a substantial layer of strongly supergradient azimuthal-mean flow between about 300-m and 2-km height near the eyewall, and a frictional asymmetry that is apparently forced by proximity to land rather than by motion. The differences between these storms will be discussed in detail, and shown to be explainable as due to the differing storm structure and motion in each case.

Corresponding author address: Dr. Jeff Kepert, Bureau of Meteorology Research Centre, GPO Box 1289K Melbourne, 700 Collins Street, Docklands, VIC 3001, Australia.
E-mail: j.kepert@bom.gov.au

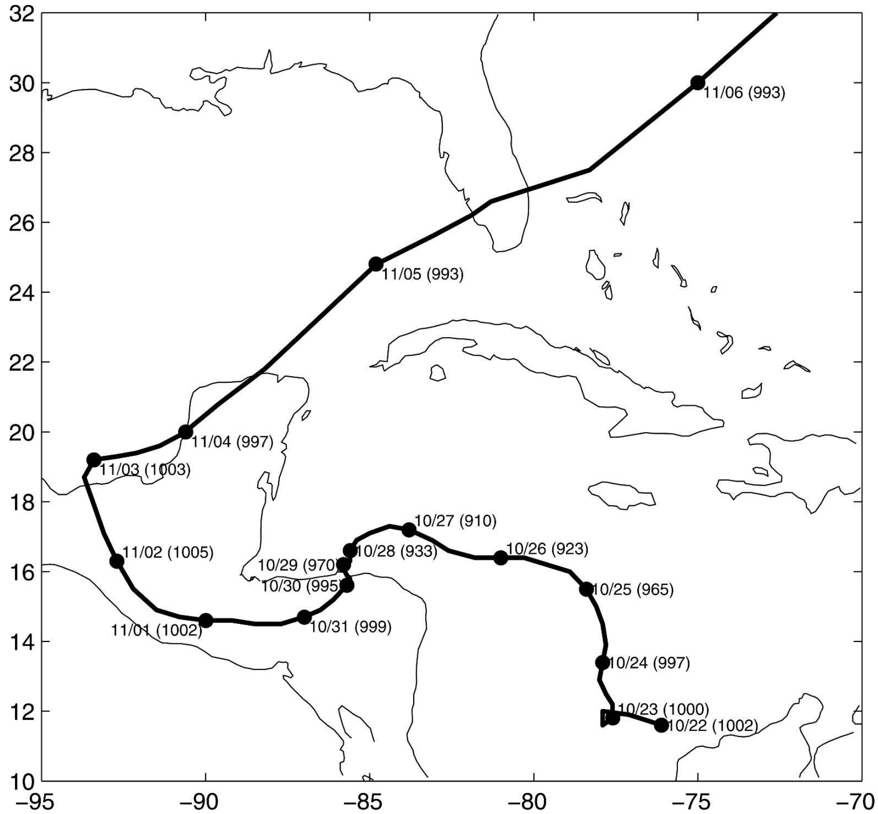

Fig. 1. The best-track analysis for Hurricane Mitch from the U.S. National Hurricane Center. Tick marks showing the month, day, and estimated central pressure (hPa) are at 0000 UTC.

The structure of this paper is as follows. The data used are described in section 2, and the BL flow analyzed in section 3. Gradient balance is diagnosed in section 4 and model simulations presented in section 5. Section 6 summarizes the conclusions and includes a detailed comparison of the two storms.

2. Synopsis and data coverage

Hurricane Mitch was one of the deadliest Atlantic hurricanes on record, with freshwater flooding following its landfall in Honduras reported to have claimed over 9000 lives. Its peak intensity was estimated by the NHC to be 155 kt with a central pressure of 905 hPa at 1800 UTC 26 October 1998, an October intensity record for the Atlantic basin, which occurred as Mitch moved steadily into the western Caribbean. Following this peak, Mitch gradually slowed, began to weaken, and eventually turned south toward the Honduras coast. The NHC best track is shown in Fig. 1, and further details may be found in Pasch et al. (2001) and Guiney and Pasch (1999).

A National Oceanic and Atmospheric Administration (NOAA) research aircraft extensively surveyed the core region of Hurricane Mitch late on 27 October, by which time the central pressure had risen to around 930 hPa and was continuing to rise. This reconnaissance occurred some 30 h before the landfall on Honduras, which was approximately 80 km to the south at the time. Mitch was moving slowly southward, and continued in this slow and at times erratic motion until landfall. A total of 10 radial legs were flown, during which 31 GPS dropsondes were deployed, all except one of which were within 100 km of the storm center. The storm-relative dropsonde launch points, and aircraft radial legs, are shown in Fig. 2.

The data used are similar to those of Part I, namely,

- thirty GPS dropsonde soundings within 100 km of the center of the storm, full details of which are in Kepert (2002c, his table 4.2);
- research aircraft measurements of three-dimensional wind, thermodynamic, and storm track data, averaged into 0.5-km radius bins for each of the ten radial legs flown, and transformed back into earth-relative coordinates for this analysis;

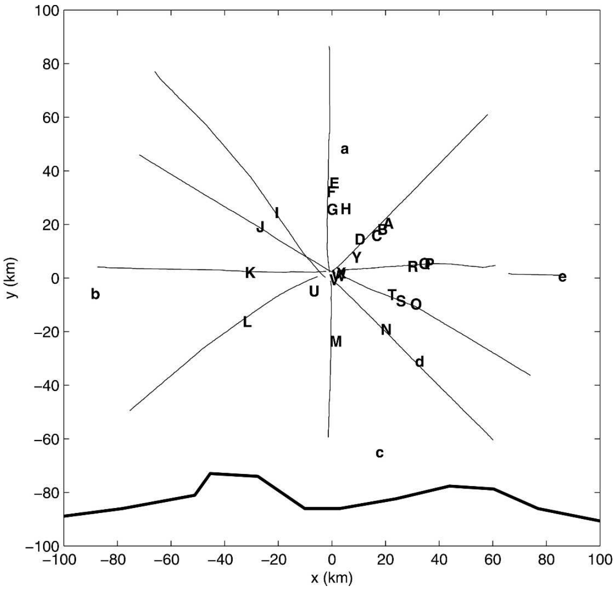

FIG. 2. The aircraft reconnaissance radial legs (light curves) and dropsonde deployment points used in this study, in storm-relative coordinates. The heavy curve to the south of the panel is the coastline of Honduras.

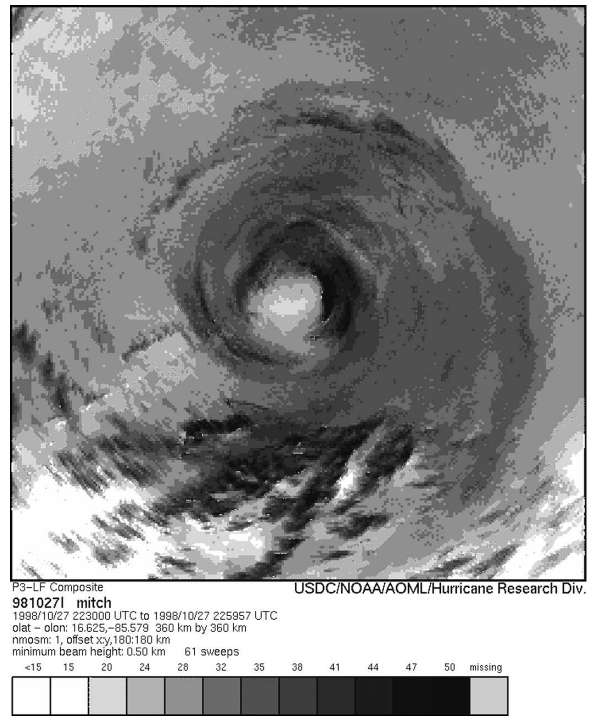

FIG. 3. Composite airborne radar reflectivity radar image for Hurricane Mitch from 2230 to 2300 UTC on 27 Oct 1998. Image courtesy of NOAA HRD.

- several composite radar images from the lower-fuselage radar on the NOAA aircraft;
- analyses of wind and geopotential height at various pressure levels from the European Centre for Medium-Range Weather Forecasts 40-yr Re-Analysis (ERA-40) project.

All times were expressed relative to a nominal base time of 2300 UTC on 27 October 1998, and dropsonde and aircraft data were navigated into a Cartesian coordinate system with origin tangent to the earth at 16.65°N, 85.567°W, the location of Mitch at this time interpolated from the NHC best-track analysis.

During the observation period, Mitch had an asymmetric appearance on radar imagery (Fig. 3), with the bulk of the eyewall convection located in the northeast, or left rear, quadrant, and an opening in the eyewall to the southwest. The surrounding stratiform rain was likewise predominantly located to the north and east. Examination of passive microwave imagery from the Defense Meteorological Satellite Program (DMSP) and Tropical Rainfall Measuring Mission (TRMM) satellites (not shown) shows that a similar asymmetry first became apparent shortly after the time of maximum intensity, and that it continued to strengthen until landfall. This asymmetry is consistent with the effects of environmental shear. Hodographs of the environmental wind (Fig. 4) show that Mitch was subject to weak vertical environmental shear from the west to northwest, from the time of peak intensity to the period analyzed here. Idealized modeling studies (Jones 1995, 2000a,b; Wang and Holland 1996; Bender 1997; Frank and Ritchie 1999, 2001; Reasor et al. 2004) have shown that the effect of shear is to produce a vortex tilt with and to the left of the shear vector, and a marked asymmetry in the eyewall vertical motion with ascent downshear left and descent opposite. The rainfall (and hence radar reflectivity) maximum in these studies occurs slightly downstream of the maximum updraft, due to the cyclonic advection of falling rain. This structure is largely consistent with the observational studies of Marks et al. (1992), Houze et al. (1992), Black et al. (2002), Reasor et al. (2000), and Corbosiero and Molinari (2002), with the latter adding that the lightning peak outside of the RMW occurs downshear right. The asymmetry in the radar reflectivity in Fig. 3 is thus qualitatively consistent with the analyzed environmental vertical shear.

However, it is not clear that this shear is sufficient to explain the intensity change. Infrared and visible satellite imagery (not shown) showed that the cirrus overcast maintained a symmetric appearance while the storm was weakening, and up until landfall. Similarly, passive microwave imagery from the TRMM and DMSP satellites showed that spiral bands were present

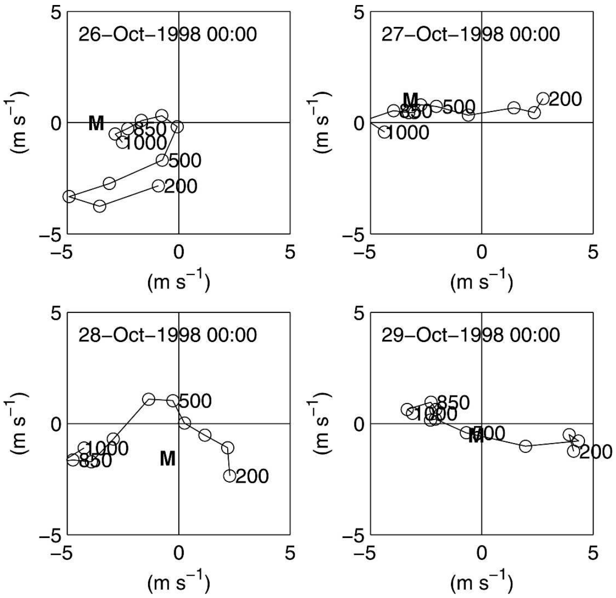

FIG. 4. Environmental wind hodographs averaged over a storm-centered 200–800-km annulus, calculated from the ERA-40 reanalysis at the times shown. The letter M shows the storm motion, according to the NHC best track, at the time.

in all sectors around the storm up until landfall, suggesting the environmental shear was relatively weak. Observational (Gallina and Velden 2002; Paterson et al. 2005) and modeling studies (Frank and Ritchie 2001; Wong and Chan 2004) have suggested that a threshold value of shear, in the vicinity of 9–10 m s^{-1} for the full-tropospheric shear, is required before weakening occurs, while the Statistical Hurricane Intensity Prediction System (SHIPS; DeMaria and Kaplan 1999) supports a similar value (J. Kaplan 2004, personal communication). The environmental shear (Fig. 4) was below this value until after the study period. Wong and Chan (2004) have shown that intense storms are more resistant to environmental vertical shear than weaker storms, and Mitch was one of the most intense Atlantic storms on record. Finally, the storm weakened steadily up until landfall in reasonably constant shear, although Frank and Ritchie's (2001) results indicate that a new equilibrium intensity would have been attained in this situation.

Another possible reason for the weakening is that, because of its slow motion, Mitch was over progressively colder water due to upwelling and mixing. Sea surface temperature observations were available from six airborne expendable bathythermographs deployed during the reconnaissance mission. Five of these recorded sea surface temperatures in the range 28° to 29°C, while one (in the southwest eyewall, near islands) reported 26.5°C (P. G. Black 1998, personal communication). These high temperatures are consistent with the climatological deep mixed layer in the Gulf of Honduras at this time of year, and seem too warm to have been a major cause of the weakening.

A further possibility is the proximity to land. Tropical cyclones weaken after landfall because the low heat capacity and conductivity of soil means that the surface heat and moisture fluxes that fuel the storm are not able to be sustained after landfall (Tuleya 1994). Usually this effect does not noticeably affect the intensity before landfall, but Mitch approached land very slowly, with the final 80 km to Honduras taking some 30 h. Thus it is possible that Mitch was affected by reduced fluxes for a relatively long while before landfall, allowing more time for the storm to respond to the reduced energy supply than is normally the case. In support of this hypothesis, consider the recent idealized BL simulations using an axisymmetric depth-averaged model of Smith (2002). He found that the BL equivalent potential temperature θ_e beneath the eyewall depended largely on the breadth of the outer wind profile, with large storms having a higher subeyewall θ_e than small ones. The amount by which the BL θ_e increased in the last 50 km or so of inflow outside of the RMW varied relatively little between the cases he considered, and so the eventual eyewall θ_e was largely determined by the value at a radius of around 100 km. Provisionally applying this idea to Mitch, a substantial part of the storm outside of this radius was over land for an unusually long period, leading to low values of BL θ_e there and hence at the eyewall. This result directly affected the intensity through the mechanisms discussed by Emanuel (1986, 1995) and Holland (1997). In support of this argument, the low-level θ_e in the dropsonde observations showed lower values in the offshore flow to the east of the storm, than to the west (not shown). This idea will not be explored further here as the main focus is on the BL wind structure. However, the effect of nearby land will be shown to have had a significant effect on the BL winds in this nearly stationary storm.

a. Hydrostatic integrations of dropsonde data

As in Part I, it was necessary to carry out the hydrostatic integrations taking account of the change of radius of each sonde as it fell. Mitch had particularly strong radial flow in some quadrants, so the differences between the surface pressure calculated by a downward integration along the slant trajectory from the aircraft and the splash pressures are quite large. The mean difference is 1.8 hPa with a standard deviation of 3.5 hPa, while individual values ranged from -6 to $+10$ hPa.

A sample fit of the radial T_v profile is shown in Fig. 5.

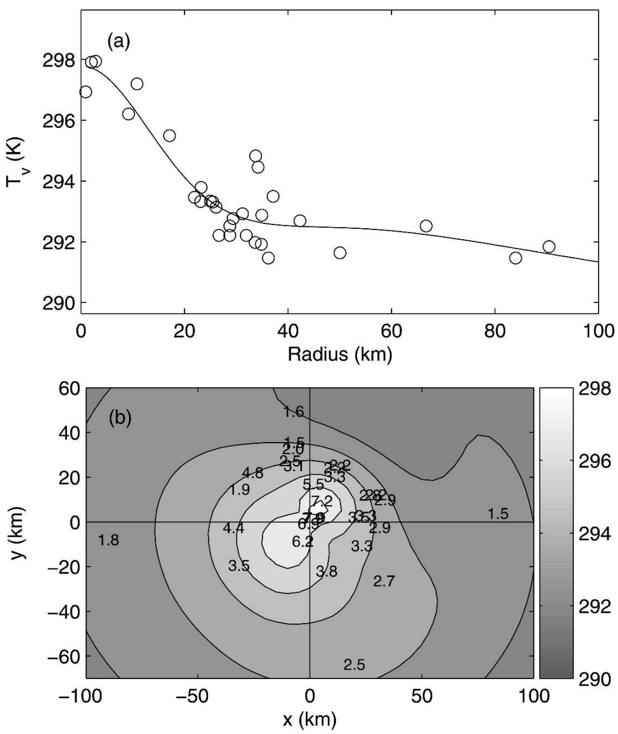

FIG. 5. (a) Observed virtual temperature at 800 hPa in Hurricane Mitch as a function of radius, together with fitted radial profile. (b) Objective two-dimensional analysis of the same data, showing the asymmetry with warm temperatures to the southwest of the center. The plotted numbers are the observations with 290 K subtracted and the contour interval is 1 K.

The top panel shows the virtual temperature observations as a function of radius and the fitted curve. There is a degree of scatter near the RMW. The same observations are plotted and analyzed in the bottom panel; the analysis was prepared by a univariate statistical interpolation method similar to that used for the wind analyses in Part I. It is clear that the warm core was displaced to the southwest of the vortex center, leading to much of the scatter near the RMW visible in the top panel. A similar asymmetry is also apparent in the flight-level temperature observations, and at other levels (not shown). This temperature asymmetry is hydrostatically consistent with the weak vortex tilt to be discussed in the next section, and is presumably a result of the subsidence on the southwest side of the TC implied by the rainfall asymmetry. Although a temperature asymmetry is present, the radial temperature gradient from the axisymmetric analysis is sufficiently accurate to correct the dropsonde virtual temperature profiles for the hydrostatic integration.

The fitted T_v curves were differentiated with respect to radius, and the temperature gradients so obtained were used to adjust each sounding to the radius of its particular hydrostatic boundary condition. The hydrostatic equation was then integrated, and the resulting profiles of height as a function of pressure were assigned to the location and time of the hydrostatic anchor point. This point was the splash position, except for two cases when this was not available and the aircraft geopotential altitude and pressure were used instead. As a consistency check for those sondes that used the near-surface measurement as their hydrostatic anchor point, downward integrations using the aircraft height and pressure (corrected for the radius change) as the boundary condition were carried out to estimate a surface pressure. The difference between this hydrostatic surface pressure estimate and the splash pressure had a mean of 0.3 hPa and standard deviation of 1.6 hPa, with values ranging from −4 to 3.5 hPa. The agreement is substantially better than obtained from uncorrected integrations along the dropsonde trajectory, and shows that the correction of the soundings for slant effects is valid.

TABLE 1. Storm tracks found by various methods for Hurricane Mitch on 27 Oct 1998. Algorithm WC82 refers to the nonlinear track from the original Willoughby and Chelmow (1982) method, TWCW to the modified Willoughby and Chelmow (1982) method to use asynoptic data and an improved observation-error specification, TMHG to the modified version of the simplex method of Marks et al. (1992) to use asynoptic data, and TPF to the translating-pressure-fit method, all as described in Kepert (2005); SR refers to storm-relative and ER to earth-relative winds, FL to aircraft flight-level data from 2118 to 2351 UTC, and SFC to dropsonde surface data from 2128 to 0031 UTC. All tracks are in a Cartesian coordinate system centered at the NHC best-track position at 2300 UTC.

Method	x_t (km)	y_t (km)	u_t (m s^{-1})	v_t (m s^{-1})
WC82	—	—	—	—
TWCW SR FL	−4.4	−3.1	−0.14	−1.53
TWCW ER FL	−3.6	−3.1	−0.23	−1.49
TMHG SR FL	−2.7	−3.9	−0.22	−1.56
TMHG ER FL	−1.9	−4.1	−0.14	−1.63
TPF FL	−2.5	−5.8	−0.2	−2.09
TPF SFC	−2.9	−7.2	−0.08	−1.96

b. Cyclone track

The cyclone track was calculated using the objective methods described in Kepert (2005), with the results shown in Table 1. The techniques using wind measurements have the track displaced to the west when storm-relative winds are used, relative to that found using earth-relative winds, but the displacement is small, consistent with the slow motion. The translating-pressure-fit (TPF) technique applied to either flight-level or dropsonde surface data located the center slightly further to the south with marginally quicker motion than any of the wind-based techniques. The slightly faster

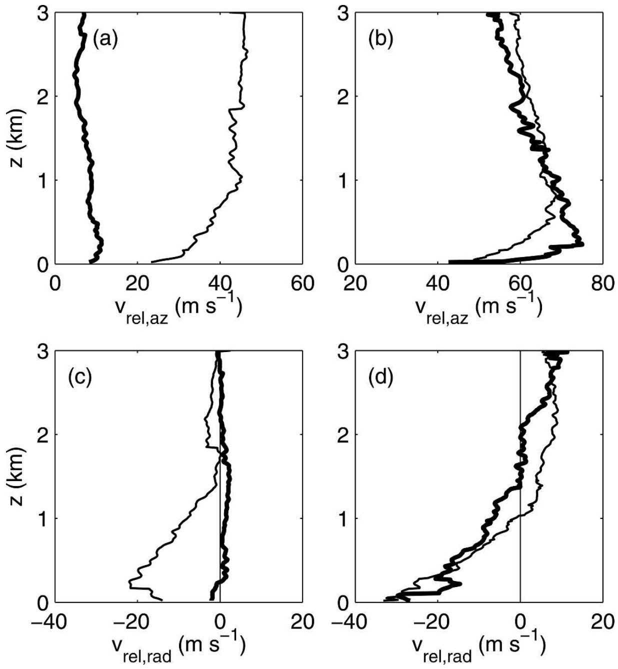

FIG. 6. (a) Mean profiles of storm-relative azimuthal wind over radius ranges 0–15 km (heavy) and 40–100 km (light). (b) As for (a), over radius ranges 15–25 km (heavy) and 25–40 km (light). (c), (d) As for (a), (b), but for the storm-relative radial wind component.

motion in this pair of tracks may be an artifact of the central pressure change of about 1 hPa h^{-1} during this period (Kepert 2005). A small northeastward tilt with height is apparent from these analyses, consistent with the environmental vertical shear. The good agreement between the different methods gives confidence in the correctness of the result. For the remainder of the study, the track found by applying the TPF method of Kepert (2005) to the flight-level wind data will be used for all coordinate transformations. The use of the other tracks does not materially affect the results.

3. The wind field

a. Radial structure

Mean profiles of storm-relative azimuthal and radial wind for the annuli 0–15 km (inner eye), 15–25 km (inner RMW), 25–40 km (outer RMW), and 40–100 km (outer core) are shown in Fig. 6. The mean azimuthal wind in the outer core is nearly constant with height above 1 km, and decreases steadily below that toward the surface. The inflow layer here is approximately 1.3 km deep. The outer RMW annulus has a marked azimuthal wind maximum at about 700-m height, while the mean inflow exceeds 30 m s^{-1} near the surface, is about 1 km deep, and lies beneath a deep layer of outflow. Immediately inside of the RMW is a very strong and sharp maximum in the azimuthal component near 250-m height. The near-surface inflow is a little weaker and deeper than on the outside of the eyewall, and similarly capped by outflow above 2 km. The eye mean sounding has nearly constant azimuthal flow with height, with a weak maximum near 250-m height, while the mean radial component is close to zero. The maximum in the azimuthal flow thus becomes more pronounced and closer to the surface inward across the eyewall, and always lies within the inflow layer, in accordance with the theory of K01 and KW01. The radial trend in inflow is similarly in agreement with the theory for the two outer annuli, but the deeper inflow on the inner side of the eyewall is contrary to the theory. The data are however unevenly distributed in azimuth, and so this anomaly may be due to insufficient sampling in the presence of a strong azimuthal asymmetry.

b. Individual profiles

Figures 7 and 8 show the storm-relative azimuthal and radial flow components, and location, measured by these dropsondes. (Model results are also shown and will be discussed later.) The data include three sets of closely spaced soundings across the eyewall, profiles A to D, E to H, and P to T. Each set shows the trend already noted, with the low-level wind speed maximum becoming more pronounced and closer to the surface toward the center of the storm. The upstream end of the most intense eyewall convection (profiles P to T) has a strong deep inflow. The inward component near the surface is around 40 m s^{-1} (or even 50 m s^{-1} if profile O is included), and the inflow layer 2 km deep at the outer end of the transect. The strength and depth of the inflow diminish toward the center of the storm, and weak outflow is apparent in the upper part of profile T.

The second transect, profiles A to D, has weaker near-surface inflow and more marked outflow aloft. A similar trend to that in profiles P to T, of decreasing inflow toward the center, can be seen in profiles A to C. Profile D represents a discontinuity here, possibly as it was taken at a different time. Less change in the jet structure, now broader and higher, is apparent along the third transect (E to H). Inflow is weak and confined close to the surface in these profiles, with a deep layer of outflow above, which increases in strength toward the center of the storm. Here as in the other transects, the radial variation of inflow implies low-level convergence.

The five profiles in the eye fall on an approximately north–south transect. The wind components from these soundings, and their positions, are shown in Fig. 9. The

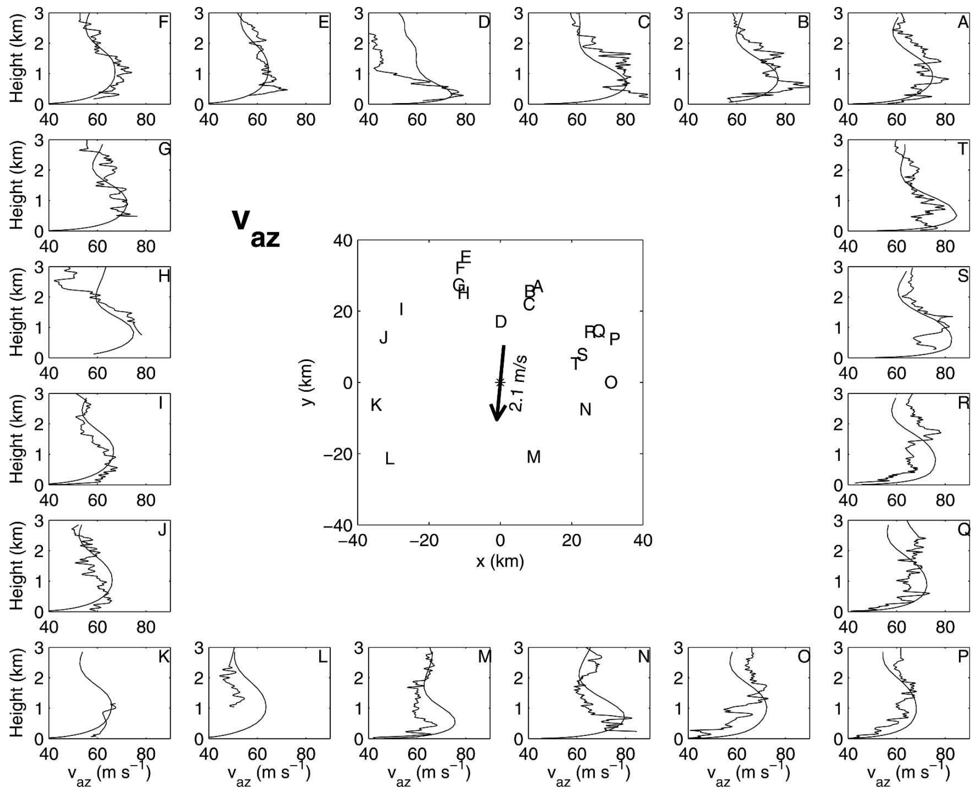

FIG. 7. Profiles of observed storm-relative azimuthal wind in Hurricane Mitch for the 20 near-eyewall dropsondes (curves with small-scale fluctuations) and represented in the model (smooth curves). The position of each sonde at 1-km height and the storm motion are shown in the central panel. The Honduras coast was approximately 80 km south of the storm center at this time.

radial flow components show a marked throughflow, with those to the south of the center exhibiting inflow, and those to the north, outflow. Profiles U and Y, at radii near 10 km, show pronounced near-surface maxima in the azimuthal component, while the remaining profiles, within a few kilometers of the center, have little in the way of coherent vertical structure. In each case the frictional BL is clearly very shallow, continuing the trend that the depth of the BL is a minimum in the center of the storm.

The five outer core wind profiles are plotted in Fig. 10. The upper part of the profiles clearly exhibit general throughflow from the east to the west, probably related to the environmental flow (Fig. 4). The three profiles (A, D, and E) to the east and north of the storm show wind speed maxima near 1-km height, which are absent from the other two. The near-surface inflow layer is strongest and deepest to the south and east of the storm, upstream of this region.

c. *Horizontal analyses*

Horizontal analyses of the wind components at various levels were prepared as in Part I and are shown in Fig. 11. The inflow is strongest near the surface to the east and decreases aloft, with outflow becoming apparent to the west from about 300-m height, and strengthening above that as the symmetric inflow weakens faster than the asymmetry. The strongest azimuthal winds occur between about 400- and 800-m height to the north of the storm. The asymmetry is wavenumber one at all levels, with no evidence of the higher wavenumber structure found in Georges. Between 500-m and 3-km height, the asymmetry rotates anticyclonically with height at 40°–60° km^{-1}, depending on which wind component is used. The azimuthal and radial-flow asymmetries are in approximate quadrature, with the azimuthal-wind maximum always downstream of the strongest inflow. The partial exception to this relationship, near the surface, is probably because the azimuthal-wind analysis has the maximum too far to the west due to a shortage of data. The storm-relative environmental flow (Fig. 4) also shows an anticyclonic rotation with height, but at a much lower rate than found here, particularly at these levels. Thus this structure is not due to the surrounding environment.

The phase relationship and anticyclonic rotation with

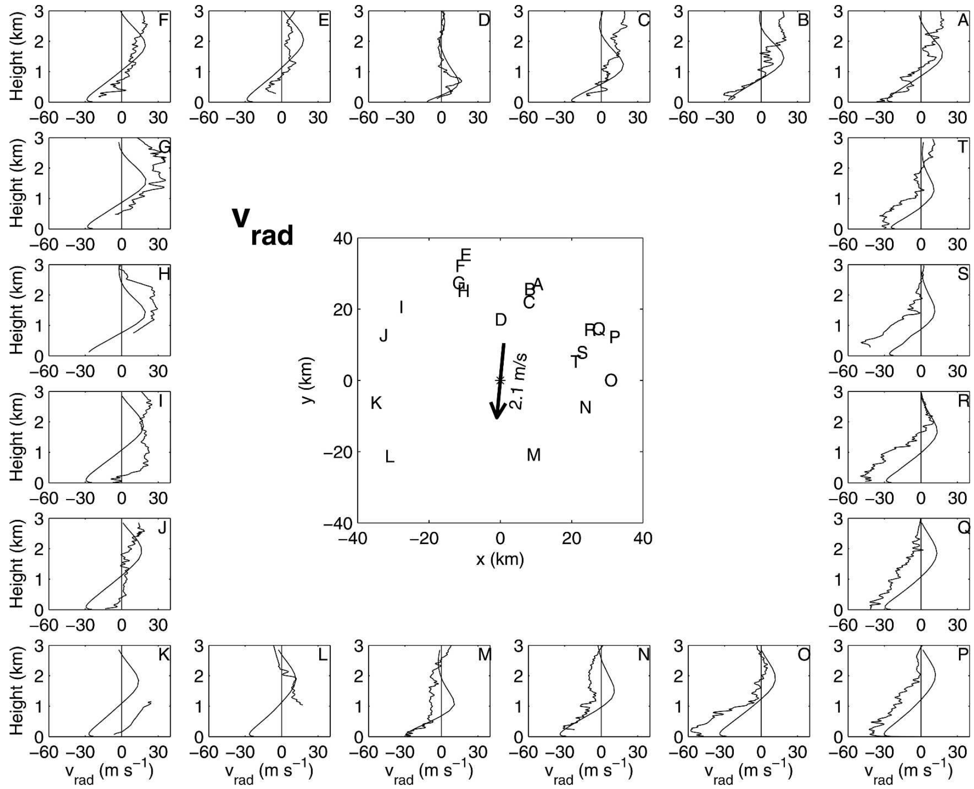

FIG. 8. Same as Fig. 7, but for storm-relative radial component.

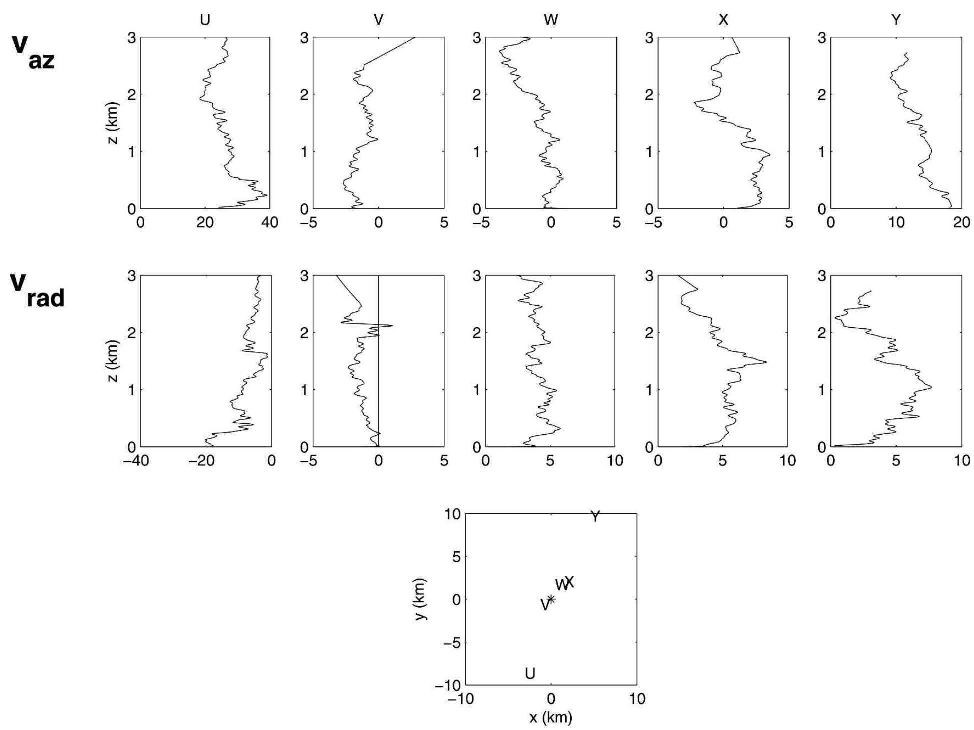

FIG. 9. Profiles of storm-relative (top row) azimuthal and (second row) radial components, for five dropsondes in the eye of Mitch. (bottom) Storm-relative positions at 1-km height are shown in alphabetical order from SSW to NNE.

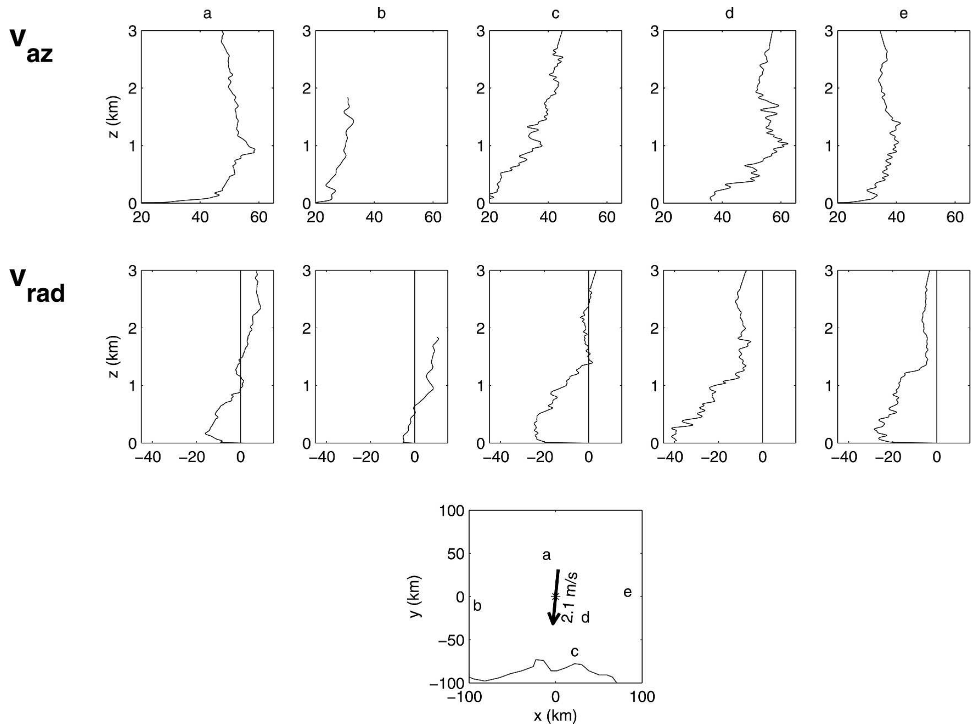

FIG. 10. The same as Fig. 9, but for profiles outside of radius 40 km. The bottom panel additionally shows the storm motion and Honduras coastline.

height of the wind components are similar to that of the dominant asymmetric component identified by K01 and shown to be equivalent to a frictionally stalled inertia wave. However, the strongest storm-relative inflow is here located in the northeast or left-rear quadrant, not the right front as his theory predicts. Thus while the vertical structure of the asymmetry suggests that frictional processes are governing the form of the asymmetry, it is clearly not being generated by the motion-induced surface-friction asymmetry. This structure will later be shown to be produced by asymmetric friction due to the proximity to land.

d. Wind reduction factor

The horizontal wind analyses were used to calculate the wind reduction factor (WRF), that is, the ratio of a near-surface earth-relative wind speed to that at some higher level. The 100-m level was used as the near-surface wind to obtain adequate data coverage. The WRF analyses, relative to the 1- and 2.5-km levels are shown in Fig. 12. From the lower level, the eye is surrounded by a near-complete ring of values below 0.9 centered about 60-km radius, with an embedded maximum to the southeast and a break to the northeast. Near and in the eye, the WRF is higher than at larger radii, except in the northern quadrant where the strongest winds in the profile are at 1-km height. The surrounding ring of low values retreats from the north of the storm with increasing height of the reference level, until by 2.5 km it cradles the storm from the south, still with the embedded minimum to the southeast. The WRF relative to this level exceeds one over a large area near the RMW (except to the southeast) and extending to the west. The general increase toward the storm center is consistent with the predictions of K01 and KW01, although the overall values are higher here because 100-m height is being used to represent the surface flow. As already noted, the asymmetry differs from the predictions of the effect of storm motion.

4. Analysis of balance

The same steps are followed as in the analysis of balance in Hurricane Georges, although the analysis is more straightforward as there is no need to divide the data into two periods, which has the further advantage that there are approximately twice as many observations and less of a data void immediately outside the RMW, than in Georges.

a. Gradient-wind balance I: Pressure to wind

The pressure form of the Willoughby et al. (2006, henceforth WDR) profile was fit to the pressure–height

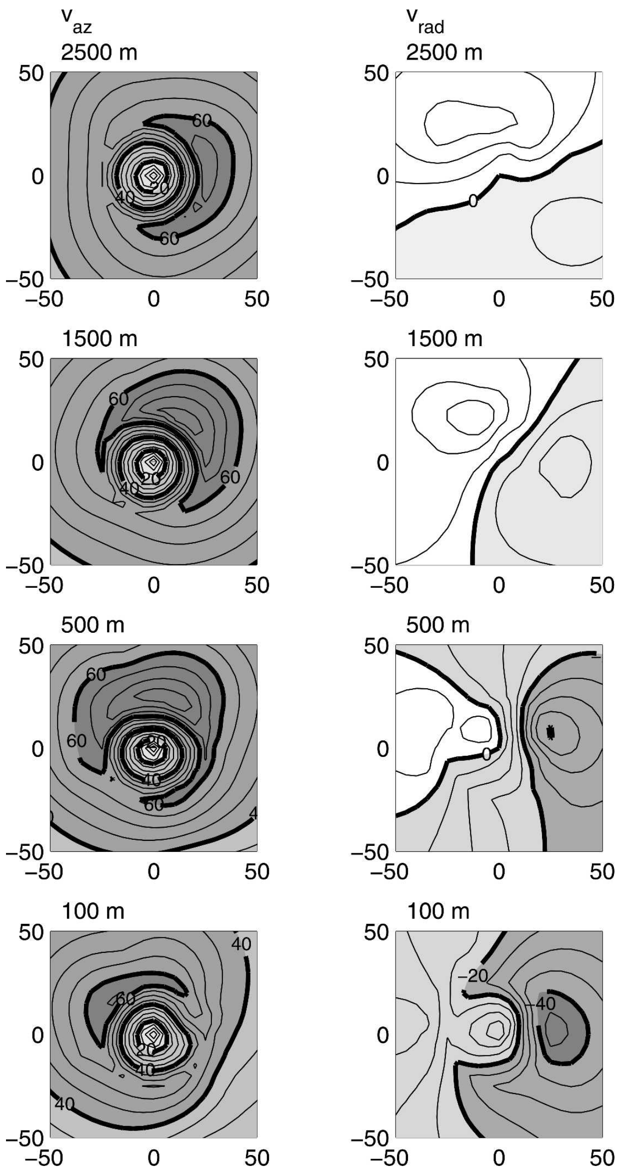

FIG. 11. Objective analyses of the storm-relative (left) azimuthal and (right) radial wind components, for levels as shown, based on dropsonde data. Contour interval is 5 m s^{-1}, with multiples of 20 m s^{-1} shown heavy. Darker shading corresponds to stronger azimuthal wind and stronger inflow, respectively.

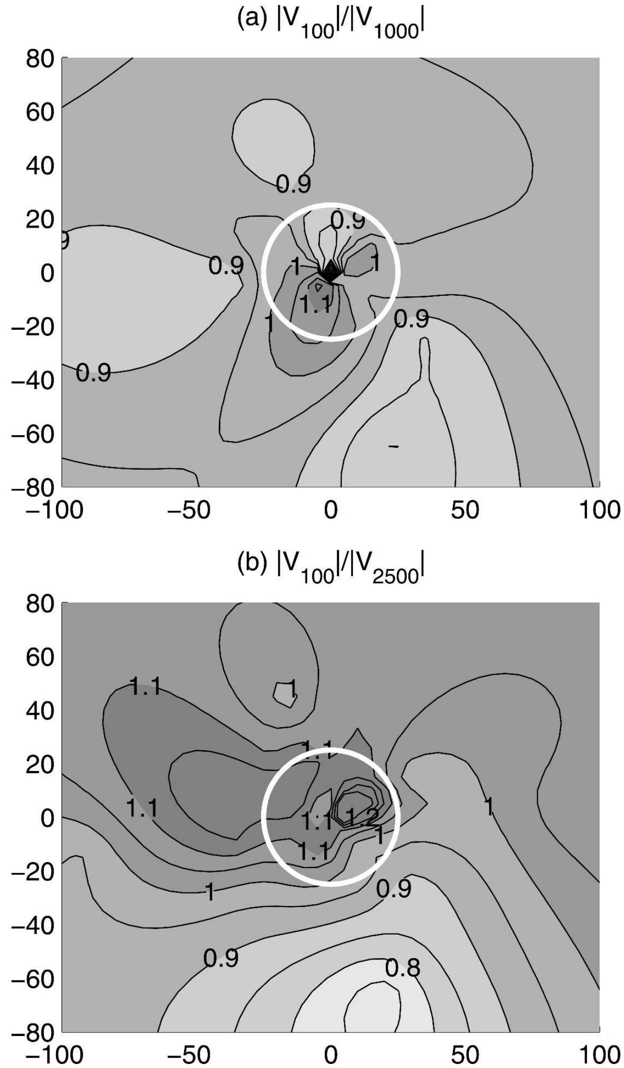

FIG. 12. Analysis of wind reduction factor, from (a) 1 km to 100 m and (b) 2.5 km to 100 m. Contour interval is 0.05, dark shading corresponds to high values, and the white circle shows the position of the RMW.

data obtained from the hydrostatic integrations, at every 100 m from the surface to 3 km. The vertical profiles of the main fitted control parameters are shown in Fig. 13. The fitted amplitude of the second outer exponential, v_{m2}, was found to be zero at all levels, in contrast to Hurricane Georges, where the wind decreased relatively slowly with radius outside the inner core. The other parameters have reasonably smooth vertical consistency, as well as a physically plausible variation with height. In particular, the maximum gradient wind speed generally decreases with height and its radius increases, as it should in a warm-cored vortex. The value of the cost function also decreases with height, at a rate that is consistent with the pressure error being proportional to pressure, rather than constant. As in Hurricane Georges, these values are possibly a reflection of the error being mainly representational; that is, due to small-scale features or asymmetries not resolved by the analysis. The pressure residuals (i.e., the difference between the observations and the fitted values) were carefully examined to check that there was no systematic variation with time, azimuth, or radius. Apart from an increase with time of about 1 hPa h^{-1}, consistent with the National Hurricane Center (NHC)-estimated weakening

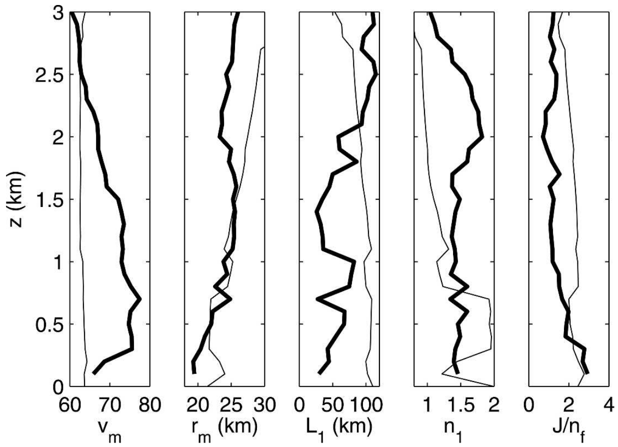

FIG. 13. Vertical profiles of control parameters for fits of the WDR profile to pressure (light lines) and wind (heavy lines) data in Hurricane Mitch: (left to right) maximum wind speed, radius of maximum winds, first length scale, eye shape parameter, cost function divided by the number of degrees of freedom.

rate at the time of 5 hPa (6 hr)$^{-1}$, there was no systematic variation in the residuals.

The data and fitted curve are shown for three representative levels in Fig. 14, together with the observed storm-relative azimuthal winds and gradient-wind speed. The majority of the near-eyewall wind observations are substantially greater than the gradient wind; that is, the flow is supergradient. This imbalance begins at about 400-m height, and is strongest at 700 m, where the mean difference between the storm-relative azimuthal observations and the gradient wind, over the 15- to 40-km annulus, is 10 m s^{-1}. It is difficult to define the top of the layer of supergradient flow, as the observed winds tend smoothly back to the estimated gradient-wind a little above 2 km, but the flow appears to be still weakly supergradient at this level.

The analyzed pressure profiles necessarily contain errors. It is necessary to estimate the pressure error and hence the gradient-wind error, to determine whether the observed winds are statistically significantly different to the gradient wind. Propagating the errors analytically is difficult because the fitted pressure profile must be differentiated to calculate the gradient wind, so to correctly propagate the errors requires not just the analysis error at any point, but also its spatial correlation. Even then, the inherent nonlinearities would make the calculation cumbersome. The nonlinear problem also makes determining the probability distribution of the gradient-wind analysis errors and the interpretation of the usual statistical tests for difference difficult. Thus, a Monte Carlo technique was adopted. The observations were perturbed with independent normally distributed noise with a zero mean and standard deviation of 1 hPa and the curve fitting done 200 times at

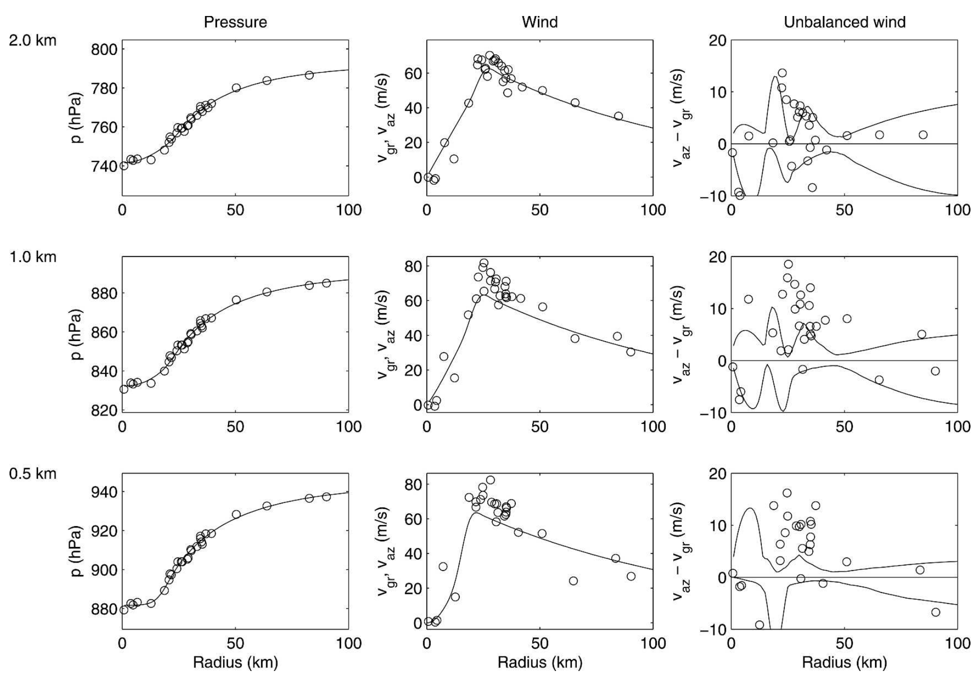

FIG. 14. (left) Dropsonde pressure observations at (top) 2 km, (middle) 1 km, and (bottom) 500 m, together with fitted profiles. (middle) Gradient-wind calculated from the pressure analyses, together with observed storm-relative azimuthal wind. (right) Difference between wind observations and the gradient wind, together with the 5th to 95th percentile confidence interval about the gradient wind.

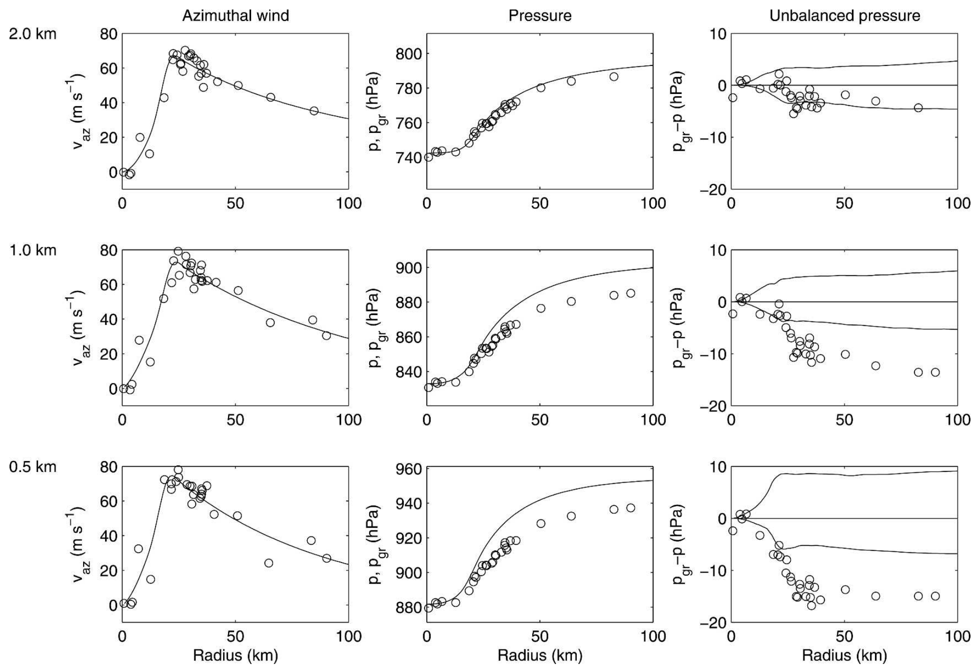

FIG. 15. Fits of the WDR wind profile at (top) 2 km, (middle) 1 k, and (bottom) 500 m, to dropsonde storm-relative azimuthal winds in Hurricane Mitch. (left) Observed and fitted winds. (middle) Pressure observations and gradient pressure curve. (right) Differences between the gradient pressure and observations, together with the 5th to 95th percentile confidence interval about the gradient pressure.

each 100-m height level. The 5th and 95th percentiles of the resulting gradient-wind estimates were then found at every 1 km of radius from the center to 100 km. Confidence intervals were used, rather than a calculation of means and standard deviations, to avoid having to make assumptions about the distribution of analysis error. The confidence bands are indicated in the right column of Fig. 14. It is clear that the wind observations lie well outside the gradient-wind confidence band at 500 m and 1 km—indeed, this is true from 400 m to 2 km. Thus the apparently supergradient flow is unlikely to be the result of chance, but is real.

b. Gradient-wind balance II: Wind to pressure

The WDR wind profile was fitted to the observed storm-relative azimuthal winds every 100 m from 100 m to 3 km. The vertical profiles of the fitted parameters are also shown in Fig. 13. There were insufficient data at large radii to reliably fit L_2, and so it were held fixed at 500 km. While the individual profiles of v_{m1} and v_{m2} are noisy, their sum varies smoothly with height and has a broad maximum between about 300 and 700 m, while the RMW also increases steadily with height.

The residuals to these fits were examined for systematic variation. An azimuthal wavenumber-1 pattern was found with amplitude about 7 m s^{-1} near the surface, decreasing to 3 m s^{-1} between 1 and 2 km, before increasing to 6 m s^{-1} at 3 km. The positive residuals were to the west at the surface, and rotated anticyclonically by about 70° km^{-1} with height. This feature is thus due to the wind asymmetry already discussed.

The boundary condition for radial integration of the gradient-wind equation was taken to be the mean observed pressure within 15 km of the TC center. The wind observations and fitted curve together with the pressure observation and gradient pressure profile for the representative levels are shown in Fig. 15, and show that the gradient-wind integration leads to an estimated pressure difference from the center to 100-km radius that is substantially below that observed at the lower two of these levels. Thus the flow is supergradient at these levels, at some radii. Overall, supergradient flow is diagnosed from 300 to 1900 m; that is, a similar height range to that found in the previous subsection, although assigning boundaries is again somewhat subjective since the flow returns smoothly to gradient balance in the upper part of the domain.

Confidence intervals for the fit were again estimated by a Monte Carlo technique. The wind observations were perturbed with random noise drawn from a normal distribution with zero mean and standard deviation

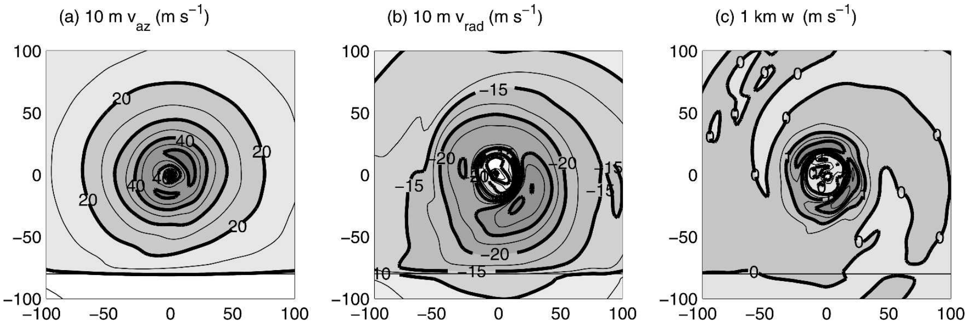

FIG. 16. The simulated storm-relative (a) 10-m azimuthal, (b) 10-m radial, and (c) 1-km vertical wind components for the model calculation of Mitch described in the text. The coastline is shown by the line at $y = -80$ km. Heavy and light contour intervals are (a) 10 and 5 m s^{-1}, (b) 5 and 2.5 m s^{-1}, and (c) 1 and 0.5 m s^{-1}.

of 5 m s^{-1}. Confidence bands defined as lying between the 5th and 95th percentiles of the derived pressure for the 200 curves are also shown in Fig. 15. The diagnosis of supergradient flow is statistically significant, to at least the 95% confidence level. In fact, between 400 m and 1 km, none of the 200 Monte Carlo fits produced as small a pressure drop from the outer core to the center, as did the observations.

As a final illustration of the imbalance, consider the vertical profiles of fitted r_m and υ_m as found by both the pressure and wind fits shown in Fig. 13. The radius of maximum winds found by the wind fits is always less than that for the pressure fits, most significantly so near the surface, while the fitted maximum wind speed is 10 m s^{-1} greater for the wind fit than the pressure fit, at and around 500 m. However, it is in agreement near the surface and above about 2.2 km. This comparison thus confirms the presence of supergradient flow near the RMW over a substantial height range. The reduction in the length scale L_1, the appearance of a nonzero υ_{m2}, and the increase in n_1, in the wind fits compared to the pressure fits, are consistent with the diagnosed region of supergradient flow being near the RMW.

5. Model simulations

Several experiments were performed with the numerical model of KW01 to see how well the observed flow could be reproduced. In these experiments, the model was forced by a WDR parametric vortex with $\upsilon_{m1} = 58.5$ m s^{-1}, $\upsilon_{m2} = 6.5$ m s^{-1}, $L_1 = 90$ km, $L_2 = 800$ km, $r_m = 25$ km, $n_1 = 0.9$, and $L_b = 10$ km translating at 2 m s^{-1}. These values are similar to those fitted using the dropsonde pressure data, apart from the addition of a small outer component with a long length scale to avoid inertial instability, and an increase in the blending width to avoid too sharp a wind maximum for the model resolution. For these calculations, the horizontal grid spacing was 3 km, and the 25 vertical levels extended from 10 m to 3.05 km with greater resolution near the surface. The first experiment did not include the effects of land and showed only a very weak asymmetry, so is not considered further.

The near-surface flow, and vertical velocity at 1-km height, from an experiment in which the cyclone approached a straight coastline behind which the land had a roughness length of 30 cm, at the moment when the land was 80 km away, are shown in Fig. 16. Significantly enhanced inflow is apparent to the southeast of the storm center, downstream of the rough land. This enhanced inflow is initially caused by the rough land, but persists over the sea downwind of the land. There is a wind speed maximum in the northeast eyewall, downstream of the enhanced inflow, while the frictionally forced updraft is strongest to the southeast, consistent with the strongest observed radar reflectivity (Fig. 3) being to the northeast, or downstream of the inflow maximum.

Azimuthal and radial wind profiles from this model calculation, interpolated to the dropsonde trajectories, were also shown in Figs. 7 and 8. The level of agreement with the observations is quite good. The transects ABCD and EFGH are well handled, with the main shortcoming being that the model-predicted structures have a shallower height scale than the observations. This height scale is sensitive to the turbulent diffusivity, inertial stability, and vertical motion, and its underprediction here is possibly due to slight misrepresentations of these parameters. Additionally, the winds aloft are too weak in the profiles inside the eye (D and H), due at least partly to the lack of a warm core in the model. Good agreement between model and observations is also found to the west of the storm, but the agreement to the south of the storm is less strong. To the east, the

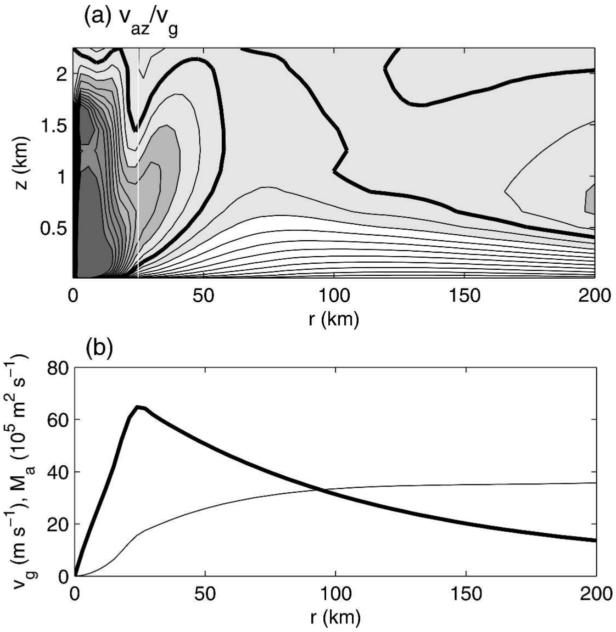

FIG. 17. (a) Radius–height section of the azimuthal mean storm-relative azimuthal wind component, divided by the gradient wind, from the model simulation of the boundary layer flow in Hurricane Mitch. Contour interval is 0.05, the contour of 1.0 is heavy, and the vertical white line shows the position of the RMW. (b) Storm-relative gradient wind speed (heavy, m s^{-1}) and absolute angular momentum (light, 10^5 m^2 s^{-1}).

inflow component in profiles O to T is generally underpredicted, possibly due to the lack of environmental shear in the model.

The major part of the observed wind asymmetry has been reproduced simply by including an area of enhanced surface friction, representing land, in the model. The modeled asymmetric vertical velocity field is also consistent with the convective asymmetry, once allowance for downstream advection is made. Earlier, it was noted that the observed wind asymmetry had structural similarities with the motion-induced frictionally stalled inertia wave discussed by K01. It seems that asymmetric surface friction, because of the proximity to land rather than to the storm motion, is indeed generating such structures here.

Figure 17 shows the azimuthal mean of the storm-relative azimuthal wind component, expressed as a fraction of the gradient wind. The model depicts the flow as being up to 20% supergradient at the radius of maximum gradient wind, with supergradient flow being present between about 200 m and 1.5 km there, and over a greater height range immediately adjacent. This result is in good agreement with the balance analysis, apart from the slight underestimate of the vertical scale by the model already noted.

6. Discussion

This two-part paper has presented detailed analyses and model simulations of the flow and gradient balance in the BL of two intense tropical cyclones. Here we summarize the results for Mitch, discuss the differences between the two storms, and the reasons for these.

Hurricane Georges was a few hours short of reaching its peak intensity, and moving quite rapidly (over 7 m s^{-1}) to the west-northwest (WNW) and well away from any land, at the time of analysis. The wind profiles around the eyewall showed a markedly asymmetric low-level jet structure, with the maximum being most marked and closest to the surface to the left of the storm. The storm-relative radial wind had a wavenumber-3 distribution below 1 km near the eyewall, with marked inflow maxima ahead of and to the right rear, and a weaker inflow maximum to the left. Above about 1 km, the wavenumber-3 pattern had vanished, and a wavenumber-1 pattern that rotated anticyclonically with height at about 40° km^{-1} was evident in both flow components. The wind reduction factor displayed considerable spatial variability, with larger values being found near the eyewall and to the left of the storm. Analysis of balance showed no evidence of supergradient flow, with the wind speeds near the eyewall being if anything slightly subgradient.[1] Simulation of the BL flow in Georges, using the model of KW01 forced by the analyzed near-surface pressure field and observed storm motion, reproduced much of the observed wind structure, but not the wavenumber-3 asymmetry. In addition, the simulated winds were only weakly supergradient near the RMW, because of the relatively flat radial profile of gradient wind at larger radii.

Hurricane Mitch was slowly weakening with the central pressure rising at about 1 hPa h^{-1}, as it moved slowly southward, during the period analyzed. It was about 80 km from the coast of Honduras at the time of the observations, but did not make landfall for another 30 h. A convective eyewall asymmetry was apparent on radar imagery, in which the southwest flank had an absence of strong convection indicating a weak or absent updraft, while the opposite prevailed to the northeast. Two-level analysis of the storm track showed that pressure center tilted slightly to the north-northeast (NNE) with height, while the warm core was displaced to the southwest. This temperature asymmetry is hydrostatically consistent with the vortex tilt, and with subsidence on the southwest side, in turn consistent

[1] Monte Carlo analyses with perturbed observations, similar to those done for Hurricane Mitch, confirm that the slight imbalances found are not statistically significant.

with the observed rainfall asymmetry. The overall structure is broadly consistent with the effects of the weak environmental shear, but it was shown using the model of Kepert and Wang (2001) that asymmetric frictional convergence in the BL due to the proximity to land also contributed to the reflectivity asymmetry.

The winds near the eyewall showed a marked low-level maximum in Mitch, which was sharper and closer to the surface toward the storm center. The radial wind showed an inflow asymmetry that rotated anticyclonically with height at about 50° km^{-1}, while the azimuthal wind had an asymmetry with similar structure, in which the strongest winds were generally about 90° of azimuth downstream of the maximum inflow at any given level. This structure is identical to the frictionally stalled inertia wave forced by asymmetric friction due to the motion of a tropical cyclone described by K01, but its orientation is not consistent with it being caused by the storm motion. Rather, it was shown by a model simulation that proximity to land was the cause. It was also speculated that the long period of being near land, due to the slow motion, may have contributed to the weakening of Mitch through reduced surface fluxes, since neither the environmental shear nor the sea surface temperatures seemed sufficient to explain the decay.

Analysis of the wind reduction factor (WRF) showed a marked increase toward the center of the storm, in good agreement with theoretical predictions, but the asymmetry was different to that predicted, since it is not dominated by motion. The WRF field is not a simple rotation of that in a moving storm as it is calculated from earth-relative winds, and the gradient wind in near-stationary Mitch is nearly symmetric.

Gradient-wind balance was diagnosed in two ways, by differentiating a pressure analysis to calculate the gradient-wind speed and comparing this to the observations, and by radially integrating the gradient-wind equation using a wind analysis, and comparing the resulting pressure field to the pressure observations. The results in either case were consistent; that the flow was supergradient between about 300 m and 2 km, with the imbalance being largest near 500 to 700 m altitude, where it reached 10 m s^{-1}. The imbalance was shown to be statistically highly significant by a Monte Carlo technique. Note also that the diagnosed return to gradient balance above 2 km is evidence for the accuracy of the analysis technique used.

The numerical model of KW01 was used to simulate a cyclone with structure similar to Mitch as it approached land. This simulation showed that the observed asymmetries in Mitch can be largely attributed to asymmetric friction due to the proximity to land, and that the extent of the supergradient flow in the model is similar to that diagnosed in the analysis of the observations. Moreover, agreement between the observed and modeled wind profiles was quite good, apart from a tendency for the model to slightly underestimate the vertical scale.

Hurricanes Georges and Mitch each displayed a very prominent low-level wind speed maximum on the inner edge of the RMW, which could be regarded as being due to the tendency for the dropsondes to fall toward the inwardly sloping RMW. While this explanation is not incorrect, it obscures the dynamics of what is happening. Above the BL, the RMW in TCs is well known to tilt with height. The flow seems to be very close to gradient balance, and the tilt can be explained using the Eliassen balanced vortex theory for the response of a balanced baroclinic vortex to thermal forcing (reviewed in Willoughby 1995), or by the thermal wind equation and the assumption of neutrality to slant moist convection (Emanuel 1986). However, the azimuthal-mean wind profiles presented show a pronounced inward migration of the strongest winds in the lowest kilometer, present in both storms but most marked in Mitch. The warm core is weakest near the surface, so this tilt cannot be due to the baroclinic effect. On the other hand, the frictional processes described by K01 and KW01 give a marked gradient in the height of the wind maximum in this area, or equivalently, a marked slope in the RMW. This feature can be seen in Fig. 2 of KW01; note that this simulation did not include a warm core. While the observed low-level wind maximum is still consistent with the sonde "falling into the eyewall," it must be recognized that the near-surface incursion of the RMW is frictionally forced. Simply describing the low-level wind maximum as the consequence of a dropsonde launched a little in from the eyewall, inevitably falling through it, fails to acknowledge the role of frictionally forced inflow in the details of the near-surface dynamics, which include supergradient flow, markedly different wind profiles on either side of the RMW, and an inwards slope of the RMW near the surface even in the absence of a warm core.

There a striking contrast in the degree to which gradient balance was diagnosed from the observations, with Mitch being very strongly supergradient, and Georges apparently not at all. This difference was successfully reproduced in the model simulations, and can be understood in terms of the quite different radial profiles of absolute angular momentum in the two storms. K01 and KW01 predicts that the jet structure in a storm is sensitive to this gradient, and that storms with a "peaked" wind profile will have a strongly supergradient jet confined to the vicinity of the RMW, while storms with a "flat" profile will have a weakly supergradient but widely distributed jet. These differences are precisely those between the radial profiles of the wind in Georges and Mitch: Georges had a steady increase in angular momentum out to large radii, while in Mitch, the angular momentum gradient was confined to the inner core and the storm was inertially near neutral at larger radii. Mitch is thus similar to KW01's Storm II, while Georges is closest to their Storm I, except that at large radii it has an even flatter wind radial profile (and consequently a stronger angular momentum gradient) than that storm. These idealized cases had respectively a strong supergradient BL jet confined close to the RMW, and a weaker but widely distributed jet. The two storms analyzed here, individually and in comparison, thus present a strong confirmation of the predictions about supergradient flow.

Both storms exhibited an increase in the WRF toward the RMW, in accordance with the predictions. In addition, Hurricane Georges showed a strong left–right asymmetry, with higher values on the left, again consistent with these predictions. Hurricane Mitch showed a marked asymmetry which is due to the proximity to land.

Hurricanes Mitch and Georges show eyewall BL wavenumber-1 wind asymmetries that are structurally similar to the frictionally stalled inertia wave discussed by K01. One difference with the theory of K01 is that there the stalled wave has a depth scale near the eyewall of about 2 km, while here the wave seems to be decaying more slowly with height than that. A possible explanation can be found by modifying K01's theory to include vertical advection, as outlined in the appendix, where it is shown that the effect of an updraft is to make the decay and oscillation scales in the Ekman-like solution unequal, with the oscillation scale increasing slightly and the decay scale increasing markedly from the no-vertical-motion case. These modifications could give rise to an anticyclonically rotating structure similar to that observed. However, the modified theory does not provide a complete explanation, as it also predicts a strong radial gradient in the height scales, which is not seen in the observations. This difference may be due to inadequate observational spatial coverage, or to horizontal mixing removing the predicted large radial gradients.

In Georges, the orientation of these asymmetries is consistent with the asymmetric friction forcing them being due to storm motion. In the case of Mitch, the very slow motion cannot be the cause, but it appears rather that proximity to land is responsible. The idea that asymmetric friction due to proximity to land can have a similar impact to that due to motion seems to be new, but is potentially of great importance since landfall is the period in the storm's life when it generally presents the greatest hazard to humanity, because of the combination of intensity and dense coastal population. Pilot studies (Kepert 2002a,b) presented simulations of the landfall of Hurricanes Danny (1997) and Floyd (1999) with encouraging agreement with observations. Note also that the observational analysis of Hurricane Frederic of 1979 by Powell (1982) showed the development of a secondary surface wind maximum on the offshore-flow side of the RMW at landfall, consistent with this process. However, it should be noted that Hurricanes Mitch and Danny represent relatively simple examples of this phenomenon, as both were very slowly moving. It is expected that the motion and landfall contributions to asymmetric friction will more commonly be of comparable magnitude, and the interaction between them may be important. Full investigation of this topic is planned.

Recently, the operational procedures for estimating surface winds from aircraft observations at the U.S. National Hurricane Center have been upgraded, based on the work of Franklin et al. (2003). Briefly, they showed from an analysis of a large number of dropsondes from 1997 to 1999 that the mean eyewall surface wind factor was larger than that at larger radii, which is clearly consistent with the predictions of K01 and KW01, and that there was also a height dependence that they attributed to the cyclone's warm core. Franklin et al.'s work is significant in that it shows that the former practice, of using the same value throughout the storm, is not appropriate. Here, consistent model results and observations demonstrate that the near-eyewall wind structure can vary greatly from storm to storm and around the eyewall of a given storm. Since there are sound dynamical reasons for these observed variations, they should be predictable. Thus there is the prospect of using either K01's or KW01's model to develop a more physically based technique for estimating the surface wind from aircraft data. This approach should offer improved accuracy over Franklin et al.'s (2003) method, since it would include details of the BL structure that these models represent reliably, even though it varies significantly with storm structure, motion, intensity, and proximity to land. Current aircraft reconnaissance strategies provide sufficient data to capture the variations in storm structure that cause the differences in BL structure, so it would be relatively easy to implement such a scheme.

Another important application could be in the use of parametric cyclone models for forcing oceanographic and risk assessment models. Such applications currently use relatively crude representations of the BL to derive the necessary near-surface winds. The good agreement between theory and observation found here implies that the models at hand would be a significant improvement.

Acknowledgments. Much of this work formed part of my Ph.D. thesis at Monash University, and I am grateful to my supervisors, Greg Holland and Dale Hess, for their encouragement and many helpful suggestions, and to my employer, the Bureau of Meteorology, for allowing me paid leave for a part of it. These analyses would have been impossible without access to the high-quality data obtained by the Hurricane Research Division (HRD) and Aircraft Operations Center (AOC) of the U.S. National Oceanic and Atmospheric Administration. I am full of admiration for the hard work and dedication of the flight and scientific crews in obtaining these data, and gratefully acknowledge the generosity of the HRD in making it so freely available. I am grateful to James Franklin and Mike Black for advice on many aspects of the GPS dropsonde, and to Hugh Willoughby and Ed Rahn for guidance on the parametric profile. The European Centre for Medium-Range Weather Forecasts kindly supplied the reanalysis data used to calculate the environmental vertical wind shears.

APPENDIX

The Effect of Vertical Advection in K01's Model

A major reason for the different results between the analytical model of K01 and the numerical model of KW01 is that the former omits vertical advection. Here, K01's solution is extended to include a crude representation of vertical advection and thereby give an improved understanding of its role. Only a sketch of the derivation is given here, since the full solution is in Kepert (2002c, section 2.5).

Restoring the vertical advection terms in K01's Eq. (6) gives

$$2\gamma\frac{\partial w}{\partial \lambda} + \frac{w}{K}\frac{\partial w}{\partial z} + 2i\sqrt{\alpha\beta}w - \frac{\partial^2 w}{\partial z^2} = 0, \qquad \text{(A1)}$$

where w is the vertical velocity and other notation is as in K01. It is not possible to solve this directly with w varying with height, but is straightforward if w is assumed to be constant. This assumption is clearly invalid near the surface, but reasonable near and above the jet. Seeking as in K01 solutions of the form

$$w(\lambda, z) = \sum_{k=-\infty}^{\infty} A_{kw}\exp(p_{kw}z + ik\lambda) \qquad \text{(A2)}$$

for complex constants A_{kw} gives equations for the p_{kw},

$$-2i(k\lambda + \sqrt{\alpha\beta}) - \frac{w}{k}p_{kw} + p_{kw}^2 = 0, \qquad \text{(A3)}$$

with solutions

$$p_{kw} = \frac{w}{2K} \pm \left[\sqrt{\sqrt{(\sqrt{\alpha\beta} + k\gamma)^2 + \frac{1}{4}\left(\frac{w}{2K}\right)^4} + \frac{1}{2}\left(\frac{w}{2K}\right)^2} + i\sqrt{\sqrt{(\sqrt{\alpha\beta} + k\gamma)^2 + \frac{1}{4}\left(\frac{w}{2K}\right)^4} - \frac{1}{2}\left(\frac{w}{2K}\right)^2}\,\right]. \qquad \text{(A4)}$$

Taking the minus sign will result in p_{kw} having a negative real part, necessary for the solution to decay with height. For simplicity, attention is restricted to the most important case $(\alpha\beta)^{1/2} + k\gamma > 0$, since the other cases are unlikely to be associated with large values of w. The decay and oscillation length scales of the solution are now different, because the real and imaginary parts of p_{kw} are unequal when $w \neq 0$. Specifically, it is straightforward to show that

$$\begin{array}{ll} |\mathrm{Re}(p_{kw})|^{-1} \geq |\,\mathrm{Im}(p_{kw})|^{-1} \geq \delta_k & w \geq 0 \\ |\mathrm{Im}(p_{kw})|^{-1} \geq \delta_k \geq |\mathrm{Re}(p_{kw})|^{-1} & w \leq 0 \end{array}, \qquad \text{(A5)}$$

with equality applying if and only if $w = 0$.

Thus, for each of the three components of the solution, the oscillation length scale $1/|\mathrm{Im}(p_{kw})|$ is always lengthened by vertical motion, while the effect on the decay scale $1/|\mathrm{Re}(p_{kw})|$ depends on the sign of w. The effect on the shape of the wind profile is to increase the strength of the supergradient flow and strengthen the outflow above it in an updraft, or to eliminate these features in a downdraft. Applying these in practice is difficult as the height scales are quite sensitive to the various parameters, including the prescribed updraft, and a real cyclone has a significant radial variation of these parameters. Moreover, the use of an azimuthally constant w may be unrealistic. Nevertheless, reasonable values of $V_m = 60$ m s^{-1}, $r_m = 25$ km, $w = 1$ m s^{-1},

$K = 50\ \mathrm{m^2\ s^{-1}}$, and $C = 0.002$ produce a rotation rate with height of the dominant $k = -1$ asymmetry of 59° km^{-1}, similar to those observed in Hurricanes Georges and Mitch. The decay scale is 19 km, so the magnitude of the predicted asymmetry is essentially constant in the levels observed.

REFERENCES

Bender, M. A., 1997: The effect of relative flow on the asymmetric structure in the interior of hurricanes. *J. Atmos. Sci.,* **54,** 703–724.

Black, M. L., J. F. Gamache, F. D. Marks Jr., C. E. Samsury, and H. E. Willoughby, 2002: Eastern Pacific Hurricanes Jimena of 1991 and Olivia of 1994: The effect of vertical shear on structure and intensity. *Mon. Wea. Rev.,* **130,** 2291–2312.

Corbosiero, K. L., and J. Molinari, 2002: The effect of vertical wind shear on the distribution of convection in tropical cyclones. *Mon. Wea. Rev.,* **130,** 2110–2123.

DeMaria, M., and J. Kaplan, 1999: An updated Statistical Hurricane Intensity Prediction Scheme (SHIPS) for the Atlantic and eastern North Pacific Basins. *Wea. Forecasting,* **14,** 326–337.

Emanuel, K. A., 1986: An air–sea interaction theory for tropical cyclones. Part I: Steady-state maintenance. *J. Atmos. Sci.,* **43,** 585–604.

——, 1995: Sensitivity of tropical cyclones to surface exchange coefficients and a revised steady-state model incorporating eye dynamics. *J. Atmos. Sci.,* **52,** 3969–3976.

Frank, W. M., and E. A. Ritchie, 1999: Effects of environmental flow upon tropical cyclone structure. *Mon. Wea. Rev.,* **127,** 2044–2061.

——, and E. A. Ritchie, 2001: Effects of vertical wind shear on the intensity and structure of numerically simulated hurricanes. *Mon. Wea. Rev.,* **129,** 2249–2269.

Franklin, J. L., M. L. Black, and K. Valde, 2003: GPS dropwindsonde wind profiles in hurricanes and their operational implications. *Wea. Forecasting,* **18,** 32–44.

Gallina, G. M., and C. S. Velden, 2002: Environmental vertical wind shear and tropical cyclone intensity change utilizing enhanced satellite derived wind information. *Extended Abstracts, 25th Conf. on Hurricanes and Tropical Meteorology,* San Diego, CA, Amer. Meteor. Soc., 172–173.

Guiney, J. L., and R. J. Pasch, 1999: Hurricane Mitch: One of the deadliest Atlantic hurricanes in history. *Mar. Wea. Log,* **43,** 4–6.

Holland, G. J., 1997: The maximum potential of tropical cyclones. *J. Atmos. Sci.,* **54,** 2519–2541.

Houze, R. A., F. D. Marks, and R. A. Black, 1992: Dual-aircraft investigation of the inner core of Hurricane Norbert. Part II: Mesoscale distribution of ice particles. *J. Atmos. Sci.,* **49,** 943–962.

Jones, S. C., 1995: The evolution of vortices in vertical shear: Initially barotropic vortices. *Quart. J. Roy. Meteor. Soc.,* **121,** 821–851.

——, 2000a: The evolution of vortices in vertical shear. II: Largescale asymmetries. *Quart. J. Roy. Meteor. Soc.,* **126,** 3137–3159.

——, 2000b: The evolution of vortices in vertical shear. III: Baroclinic vortices. *Quart. J. Roy. Meteor. Soc.,* **126,** 3161–3185.

Kepert, J. D., 2001: The dynamics of boundary layer jets within the tropical cyclone core. Part I: Linear theory. *J. Atmos. Sci.,* **58,** 2469–2484.

——, 2002a: The impact of landfall on tropical cyclone boundary layer winds. *Extended Abstracts, 25th Conf. on Hurricanes and Tropical Meteorology,* San Diego, CA, Amer. Meteor. Soc., 335–336.

——, 2002b: Modelling the tropical cyclone boundary layer windfield at landfall. *Extended Abstracts, 14th BMRC Modelling Workshop: Modelling and Predicting Extreme Events,* Melbourne, Australia, 81–84.

——, 2002c: The wind-field structure of the tropical cyclone boundary-layer. Ph.D. thesis, Monash University, Melbourne, Australia, 350 pp.

——, 2005: Objective analysis of tropical cyclone location and motion from high density observations. *Mon. Wea. Rev.,* **133,** 2406–2421.

——, 2006: Observed boundary layer wind structure and balance in the hurricane core. Part I: Hurricane Georges. *J. Atmos. Sci.,* **63,** 2169–2193.

——, and Y. Wang, 2001: The dynamics of boundary layer jets within the tropical cyclone core. Part II: Nonlinear enhancement. *J. Atmos. Sci.,* **58,** 2485–2501.

Marks, F. D., R. A. Houze, and J. F. Gamache, 1992: Dual-aircraft investigation of the inner core of Hurricane Norbert. Part I: Kinematic structure. *J. Atmos. Sci.,* **49,** 919–942.

Pasch, R. J., L. A. Avila, and J. L. Guiney, 2001: Atlantic hurricane season of 1998. *Mon. Wea. Rev.,* **129,** 3085–3123.

Paterson, L. A., B. N. Hanstrum, N. E. Davidson, and H. C. Weber, 2005: Influence of environmental vertical wind shear on the intensity of hurricane-strength tropical cyclones in the Australian region. *Mon. Wea. Rev.,* **133,** 3644–3660.

Powell, M. D., 1982: The transition of the Hurricane Frederic boundary-layer wind fields from the open Gulf of Mexico to landfall. *Mon. Wea. Rev.,* **110,** 1912–1932.

Reasor, P. D., M. T. Montgomery, F. D. Marks Jr., and J. F. Gamache, 2000: Low-wavenumber structure and evolution of the hurricane inner core observed by airborne dual-Doppler radar. *Mon. Wea. Rev.,* **128,** 1653–1680.

——, ——, and L. D. Grasso, 2004: A new look at the problem of tropical cyclones in vertical shear flow: Vortex resiliency. *J. Atmos. Sci.,* **61,** 3–22.

Smith, R. K., 2002: A simple model of the hurricane boundary layer. *Quart. J. Roy. Meteor. Soc.,* **128,** 1–20.

Tuleya, R. E., 1994: Tropical storm development and decay: Sensitivity to surface boundary conditions. *Mon. Wea. Rev.,* **122,** 291–304.

Wang, Y., and G. J. Holland, 1996: Tropical cyclone motion and evolution in vertical shear. *J. Atmos. Sci.,* **53,** 3313–3332.

Willoughby, H. E., 1995: Mature structure and evolution. *Global Perspectives on Tropical Cyclones,* R. L. Elsberry, Ed., WMO Rep. TCP-38, 21–62.

——, and M. Chelmow, 1982: Objective determination of hurricane tracks from aircraft observations. *Mon. Wea. Rev.,* **110,** 1298–1305.

——, R. W. R. Darling, and M. E. Rahn, 2006: Parametric representation of the primary hurricane vortex. Part II: A new family of sectionally continuous profiles. *Mon. Wea. Rev.,* **134,** 1102–1120.

Wong, M. L. M., and J. C. L. Chan, 2004: Tropical cyclone intensity in vertical winds shear. *J. Atmos. Sci.,* **61,** 1859–1876.